Accepted Manuscript

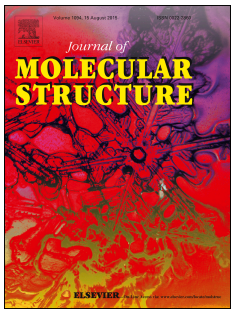

Synthesis, NMR data and theoretical study of semi-synthetic derivatives from trans-dehydrocrotonin

Breno Almeida Soares, Maria Aparecida Medeiros Maciel, Rosane Nora Castro, Carlos R. Kaiser, Caio Lima Firme

PII: S0022-2860(15)30533-0

DOI: 10.1016/j.molstruc.2015.12.045

Reference: MOLSTR 22079

To appear in: *Journal of Molecular Structure*

Received Date: 16 November 2015

Revised Date: 16 December 2015

Accepted Date: 16 December 2015

Please cite this article as: B.A. Soares, M.A. Medeiros Maciel, R.N. Castro, C.R. Kaiser, C.L. Firme, Synthesis, NMR data and theoretical study of semi-synthetic derivatives from trans-dehydrocrotonin, *Journal of Molecular Structure* (2016), doi: 10.1016/j.molstruc.2015.12.045.

Highly stereospecific hydrogenation of *t*-DCTN to form bioactive naturally found *t*-CTN.

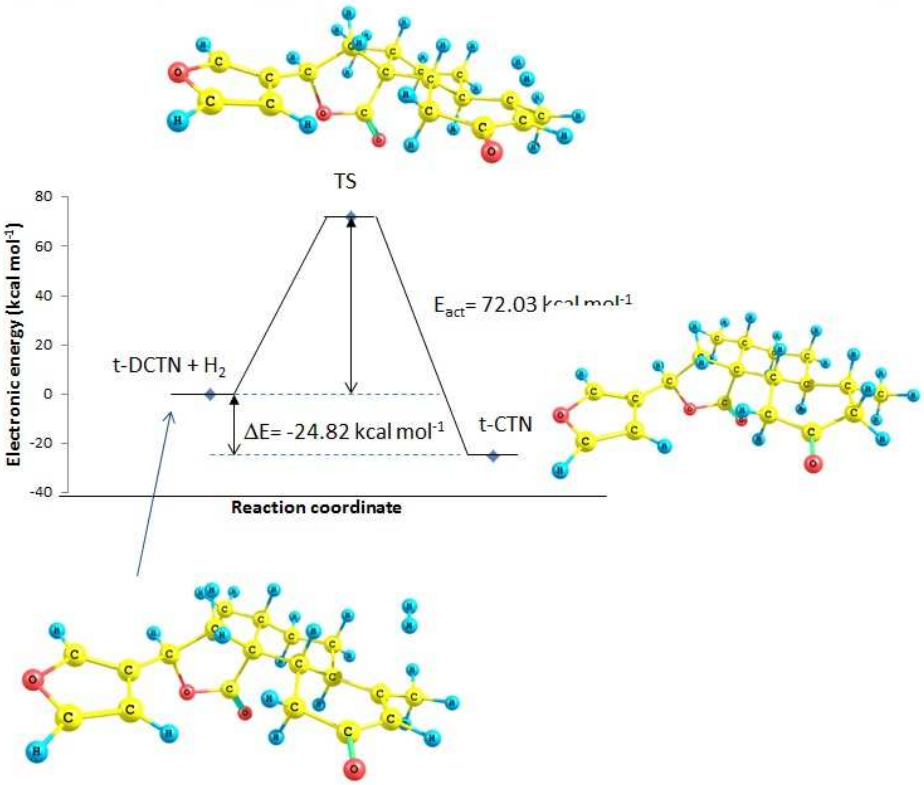

Synthesis, NMR data and theoretical study of semi-synthetic derivatives from *trans*-dehydrocrotonin

Breno Almeida Soares[a], Maria Aparecida Medeiros Maciel[a, b], Rosane Nora Castro[c], Carlos R. Kaiser [d] and Caio Lima Firme[a, *]

[a] Universidade Federal do Rio Grande do Norte, Instituto de Química, Campus Lagoa Nova, Natal-RN, Brazil

[b] Universidade Potiguar Laureate International Universities, Programa de Pós-graduação em Biotecnologia, Campus Salgado Filho, Natal-RN, Brazil

[c] Universidade Federal Rural do Rio de Janeiro, Instituto de Química, Seropédica-RJ, Brazil

[d] Universidade Federal do Rio de Janeiro, Instituto de Química, Ilha do Fundão, Rio de Janeiro-RJ, Brazil

***** Author to whom correspondence should be addressed; E-Mail: firme.caio@gmail.com or caiofirme@quimica.ufrn.br Tel.: +55-84-32119224

Received: / Accepted: / Published:

Abstract: In this work, the 19-*nor*-diterpenoid clerodane-type dehydrocrotonin (*t*-DCTN) was a primary source for a two-step synthetic procedure. The catalytic hydrogenation of *t*-DCTN afforded the semi-synthetic *trans*-crotonin (*t*-CTN) in a highly stereospecific reaction confirmed by DFT calculations. The unsaturated carbonyl group of *t*-DCTN was reduced by $NaBH_4$/EtOH providing an epimeric α-OH and β-OH mixture named *t*-CTN-OL. Both epimeric compound structures *t*-CTN-α-OL and *t*-CTN-β-OL were elucidated by 1D and 2D NMR spectral data. Comparison of NMR data from natural source of *t*-CTN was done to confirm the stereochemical authenticity of semi-synthetic *t*-CTN. Calculated NMR data for all described derivatives (semi-synthetic *t*-CTN and its *t*-CTN-OL epimeric mixture) were performed using B3LYP/6-311G++(d,p) level of theory which validated our previously developed NMR theoretical protocol for structural analyses of organic molecules. Topological data using Quantum Theory of Atoms in Molecules (QTAIM) of *t*-CTN quantified and qualified intramolecular interactions of its most stable conformer.

Keywords: *t*-DCTN; *t*-CTN; *t*-CTN-OL; NMR; QTAIM; DFT

---

1. Introduction

Crotonin (CTN), a 19-*nor*-diterpenoid clerodane, was first isolated in 1967 from *Croton lucidus* L [1] and structural elucidation beyond chemical transformations was not enough to determine the stereochemistry of the decalin moiety [2]. The absolute configuration achieved by X-ray diffraction analysis defined the *cis*-decalin junction (*c*-CTN) [3]. Sequentially, *c*-CTN semi-synthetic derivatives were prepared from the natural 15,16,-epoxy-19-*nor*-2-oxo-13(16),14-clerodadien-20,12-olide (*c*-CTN) [3]. The diastereoisomer *trans*-crotonin (*t*-CTN) was isolated from *Croton cajucara* Benth (Euphorbiaceae), an Brazilian Amazonian plant, which bark showed to be a rich source of bioactive clerodanes, among them *trans*-crotonin (*t*-CTN) and *trans*-dehydrocrotonin (*t*-DCTN) [4,5]. Since then, *t*-CTN has been described to present a few biological activities such as antitumoral [5], antiulcerogenic [6], anti-inflamatory and antinociceptive [7]. The semi-synthetic *t*-CTN was already described from the *t*-DCTN reactant by using catalytic hydrogenation process [4] and more recently its structure was target of total synthesis [8] as well as *t*-DCTN reductions [9–11].

In this present work *t*-DCTN was source for a highly stereoselective synthetic procedure affording the semi-synthetic *t*-CTN and the unknown 15,16-epoxy-19-*nor*-2-OL-13(16),14-clerodadien-20,12-olide derivatives (an epimeric mixture named *t*-CTN-α-OL and *t*-CTN-β-OL). The analysis of ^{1}H NMR showed major amount for *t*-CTN-α-OL, in a 2.81(α-OH):1(β-OH) proportion. NMR theoretical protocol previously developed for structural analyses of organic molecules confirmed structures assignments [12].

2. Experimental

2.1. General equipment

Melting points were determined in a capillary with a Melt-Temp. ^{1}H and ^{13}C NMR were recorded at room temperature using a Bruker-DRX 400 MHz spectrometer, employing

tetramethylsilane (TMS) as internal reference. The chemical shifts (δ) are given in ppm and coupling constants (J) in Hertz. The ^{1}H and ^{13}C NMR spectra for semi-synthetic *t*-CTN and epimeric mixture of *t*-CTN-OL can be viewed in Figures S1-S5. Mass spectra were obtained at 70 eV on a Shimadzu-CG/MS QP 2000A equipped with a solid probe. The mass spectra for semi-synthetic *t*-CTN and epimeric mixture of *t*-CTN-OL can be viewed in Figures S6 and S7. Fragments were described as *m/z* ratio. Thin layer chromatography (TLC) was carried out on silica gel plates with a fluorescence indicator F_{254} (0.2 mm, E. Merck); the spots were visualized in UV light (254 nm). Column chromatography was performed on silica using Kieselgel 60 (230–400 mesh, E. Merck). All solvents and reagents used in the present study were of analytical grade.

2.2. Material and Methods

Plant material was collected in Jacundá, Pará state (Amazonian region-Brazil) and identified by Nelson A. Rosa. A voucher specimen (no. 247) has been stored in the Herbarium of the Museu Paraense Emílio Goeldi (Belém-Brazil). The isolation of *t*-DCTN was performed according to the literature [4]. For semi-synthetic *t*-CTN and for epimeric mixture of *t*-CTN-OL the assignments were determined from ^{1}H (400 MHz) and ^{13}C (100 MHz) NMR equipment. The previous assignments for structure elucidation of the natural *t*-CTN were determined from ^{1}H (600 MHz) and ^{13}C (150 MHz) NMR equipment [13] which were used in a comparative structural analysis between natural *t*-CTN and the semi-synthetic *t*-CTN as well as for the epimeric mixture of *t*-CTN-OL. Assignments for semi-synthetic *t*-CTN, *t*-CTN-α-OL and *t*-CTN-β-OL were determined from ^{1}H (400 MHz) and ^{13}C (100 MHz) NMR equipment.

2.3. Synthetic Procedures

2.3.1. Synthesis of 15,16-epoxy-19-*nor*-2-oxo-13(16),14-clerodadien-20,12-olide (*t*-CTN)

In a 5 mL round bottom flask containing 30 mg of powdered *t*-DCTN solubilized in 1 mL of ethanol, a catalytic amount of charcoal over palladium was added. A yellow balloon containing $H_{2(g)}$

was adapted as showed in Figure S8. The atmosphere of reaction media was saturated with $H_{2(g)}$ three times with the aid of a needle adapted in a vacuum system. Afterwards, the system was stirred during 1 hour and half. The total consumption of *t*-DCTN could be observed using thin layer chromatography analysis in a hexane:ethyl acetate (1:1) as eluted solvent. The reaction mixture was diluted with 5 mL of ethyl acetate and filtered, the supernatant was then concentrated in vacuum to afford 23 mg (76%) of semi-synthetic *t*-CTN in form of white solid. Mp = 129-131 ºC. ^{1}H NMR ($CDCl_3$, 400 MHz): δ 7.45 (2H, m, H-15, H-16); 6.38 (1H, t, *J*=1.28 Hz, H-14); 5.41(1H, t, *J*=8.62 Hz, H-12); 2.49 (1H, tt, *J*=13.05 ; 2.65 Hz, H-1e); 2.42 (1H, dd, *J*=13.05; 8.62 Hz, H-11a); 2.32 (1H, t, *J*=8.68 Hz, H-11b); 2.36 (1H, ddd, H-3e); 2.20-2.13 (2H, m, H-1a, H-3a); 1.48-1.38 (1H, m, H-4); 2.05 (1H, dddd, *J*=11.07; 10.64; 10.58; 3.80, H-5); 2.20-2.13 (1H, m, H-6e); 1.76 (1H, dddd, *J*=13.08; 13.02; 12.75; 3.40 Hz, H-7a); 1.59 (1H, m, H-7e); 1.67 (1H, m, H-8); 1.51-1.44 (1H, m, H-10); 1.15 (3H, d, *J*=6.72, Me-17); 1.06 (3H, d, *J*=6.48, Me-18); 0.94 (1H, dddd, *J*=13.08; 12.53; 3.66 Hz, H-6a). ^{13}C NMR ($CDCl_3$, 100 MHz): δ 209.53 (C, C-2); 177.02 (C, C-20); 144.26 (C, C-15); 139.33 (C, C-16); 125.17 (C, C-13); 108.04 (C, C-14); 72.32 (C, C-12); 52.34 (C, C-9); 49.79 (C, C-3); 48.43 (C, C-10); 43.32 (C, C-1); 42.19 (C, C-8); 41.65 (C, C-5); 40.95 (C, C-11); 38.60 (C, C-4); 29.70 (C, C-6); 29.44 (C, C-7); 19.67 (C, Me-18); 17.73 (C, Me-17). EIMS *m/z* 316 $[M]^+$ (20), 204 $(M-61)^+$ (30), 121 (45), 94 (100), 81 (40), 55 (30), 41 (30).

2.3.2. Synthesis of 15,16-epoxy-19-*nor*-2-OL-13(16),14-clerodadien-20,12-olide (*t*-CTN-OL) (epimeric mixture)

The natural or semi-synthetic *t*-CTN (120 mg, 0.378 mmol) was dissolved in 5 mL of ethanol. $NaBH_4$ (14.4 mg, 0.378 mmol) was added slowly, with stirring. A gas evolution occurs, together with a temperature rise (40 ^{o}C). Stirring was continued for 30 minutes before pH was adjusted to neutrality with dilute H_2SO_4, followed by turbidity of reaction media. Then 20 mL of distilled water was added to proceed extraction with chloroform (3x15 mL). The organic phase was dryed with $NaSO_4$ and finally the solvent evaporation afforded 75 mg (63%) of crude material (pale amorphous solid). Mp =

130-132 ºC. ^{1}H NMR ($CDCl_3$, 400 MHz): δ 7,47 (2H, m, H-15, H-16); 3.59-3.52 (1H, m, H-2); 2.45-2.38 (4H, m, H-1e, H-3e, H-11a, H-11b); 2.10-2.03 (3H, m, H-1a, H-3a, H-5); 1.97-1.88 (1H, m, H-6e); 1.67-1.51 (3H, m, H-7e, H-8, H-10); 1,37-1,26 (1H, m, H-4). *t*-CTN-α-OL absorptions: δ 6.43 (1H, m, *J*=0.63 Hz, H-14); 5.40 (1H, t, *J*=8.80 Hz, H-12); 4.18 (1H, OH); 2.10-2.03 (1H, m, H-6a); 1.74 (1H, dddd, *J*=13.00; 12.72; 12.68; 3.44 Hz, H-7a); 1.12 (1H, d, *J*=6.72 Hz, Me-17); 0.98 (1H, d, *J*=5.76 Hz, Me-18). *t*-CTN-β-OL absorptions: δ 6.41 (1H, t, *J*=1.28 Hz, H-14); 5.39 (1H, t, H-12); 3.50 (1H, OH); 1,79-1.69 (1H, m, H-7a); 1.11 (1H, d, *J*=6.76 Hz, Me-17); 0.92 (1H, d, *J*=6.36 Hz, Me-18) 0,83 (1H, dddd, *J*=13.02; 12.56; 12.60; 3.60, H-6a). ^{13}C NMR ($CDCl_3$, 100 MHz): δ 177.44 (C, C-20); 144.06 (C, C-15), 139.80 (C, C-16), 125.55 (C, C-13), 108.20 (C, C-14), 72.11 (C, C-12); 51.87 (C, C-9), 46.79 (C, C-10), 44.71 (C, C-3), 42.25 (C, C-8), 41.75 (C, C-5), 41.61 (C, C-11), 29.98 (C, C-6), 29.53 (C, C-7), 19.42 (C, C-18), 17.79 (C, C-17). *t*-CTN-α-OL absorptions: δ 70.09 (C, C-2); 37.17 (C, C-1); 36.22 (C,C-4); *t*-CTN-β-OL absorptions: δ 66.69 (C, C-2); 34.18 (C, C-1); 31.85 (C,C-4). EIMS: *t*-CTN-α-OL *m/z* 318 $[M]^+$ (60), 255 (80), 206 (20), 161 (100), 105 (40), 94 (20), 81 (20), 55 (20). *t*-CTN-β-OL *m/z* 318 $[M]^+$ (5), 206 (40), 161 (50), 105 (35), 95 (100), 81 (30), 55 (20).

3. Computational details

The geometry of the studied species was optimized by using standard techniques [14]. Vibrational analysis on the optimized geometries of selected points on the potential energy surface (PES) was carried out to determine whether the optimized geometry of *t*-DTCN and *t*-CTN were true minimum or a transition state by checking the existence of imaginary frequencies. No imaginary frequency was obtained confirming that it was found a minimum in the PES for these molecules. The calculations were performed at B3LYP/6-311G++(d,p) for the optimized structures (*t*-DCTN, *t*-CTN, *t*-CTN-β-OL and *t*-CTN-α-OL), in gas phase, and ωB97XD/6-31G++(d,p) [15–20] for transition states, with implicit solvatation approach based on IEFPCM model [21,22]. The IRC calculation (see Figure 1B) was performed at B3LYP/6-31G++(d,p) level of theory. All calculations were done by

using GAUSSIAN 09 package [23]. The electronic density of *t*-CTN was obtained from the optimization of the Kohn-Sham orbitals from the optimized structure of *t*-CTN for further calculation of the corresponding molecular graph and atomic integrations of the hydrogen atoms in order to obtain the delocalization index between vicinal or long range hydrogen atoms. Topological data were calculated using AIM2000 software [24].

4. Results and discussions

Semi-synthetic *t*-CTN was obtained from *t*-DCTN using an alternative apparatus for the catalytic hydrogenation, in which a balloon containing hydrogen gas assisted by a vacuum system allowed the necessary saturated atmosphere to reduce the decalin double bond ($\Delta^{3,4}$ unsaturation) (Scheme 1). TLC analysis confirmed a quantitative conversion of *t*-DCTN into *t*-CTN, being in agreement with our previously applied methodology [4].

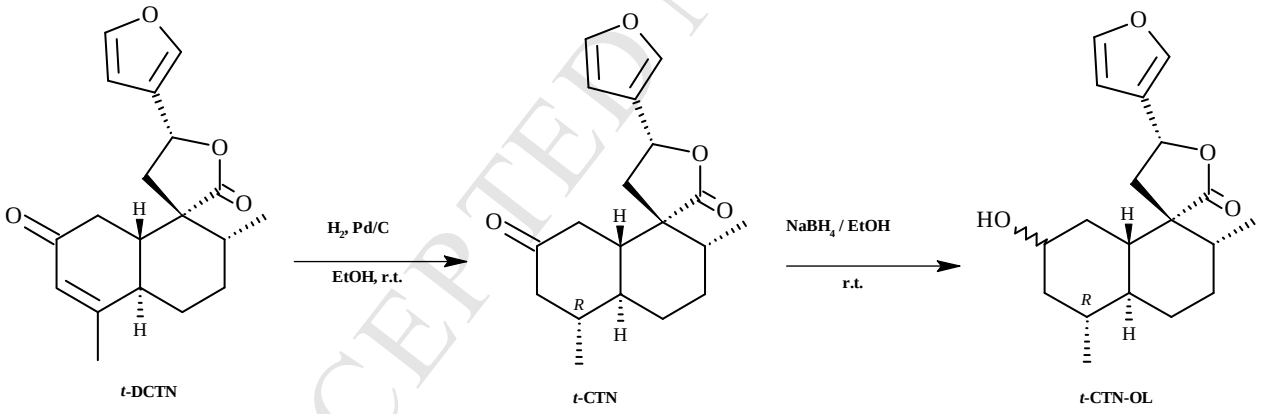

Scheme 1. Preparation of *t*-CTN-OL epimeric mixture.

A comparative structural analysis between natural *t*-CTN and the semi-synthetic *t*-CTN confirm reaction high stereospecificity as well as C-4 asymmetric center configuration. Semi-synthetic *t*-CTN and natural *t*-CTN (previously analyzed by 600 MHz field [13]) showed great data correlation. For this synthesis, theoretical calculation was applied and since modeling the heterogeneous catalysis with Pd/C is not feasible due to the amorphous nature of activated charcoal, we opted for theoretical

calculation without catalyst. From DFT calculation (B3LYP/6-311G++(d,p) level of theory), it was observed that hydrogen attack to *Re* face of *t*-DCTN decalin double bond has 72.03 kcal mol^{-1} non-catalyst energy barrier (Figure 1A). The corresponding transition state is confirmed by intrinsic reaction coordinate calculation (IRC) at B3LYP/6-31G++(d,p) level of theory (Figure 1B), represented by the non-optimized *t*-CTN (I) and *t*-DCTN-H_2 complex (III), plus optimized TS (II).

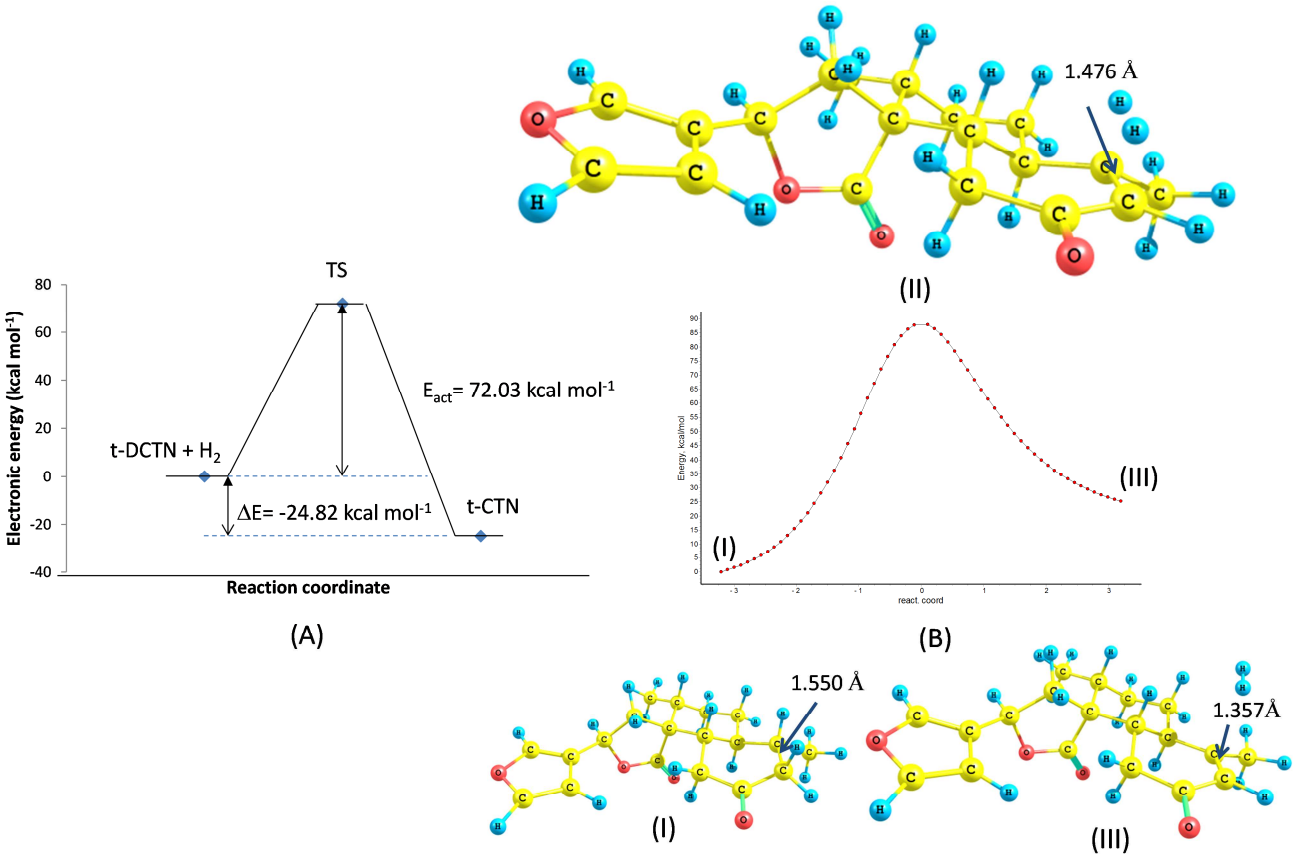

Figure 1. (A) Pictorial representation of potential energy surface of hydrogenation reaction of *t*-DCTN decalin double bond according to corresponding optimized geometries of reactants, transition state and product; (B) IRC calculation from transition state (II) of hydrogenation of *t*-DCTN (III) forming *t*-CTN (I).

On the other hand, no corresponding TS structure from hydrogenation reaction at *Si* face of *t*-DCTN decalin double bond was found from B3LYP calculation. In Figure 2A it is depicted one out of several starting geometries (from previously optimized *t*-DCTN and hydrogen isolated molecules) in

order to find the corresponding TS. Nonetheless, another transition state was found (Figure 2B) in which a new pair of saturated carbon atoms (C-3 and C-4) is formed; the former covalent bond from bridgehead carbon atoms of decalin moiety (C-5 and C-10) is cleaved; and C5–H bond is partly broken. The corresponding TS imaginary frequency indicates the proton transfer from C-5 to C-10 in order to form a carbene derivative (Figures 2C and 2D). The energy barrier for this transition state is 89.49 kcal mol^{-1}. One important consequence of this result is that the high stereoespecificity of hydrogenation of *t*-DCTN is independent of the Pd/C catalyst.

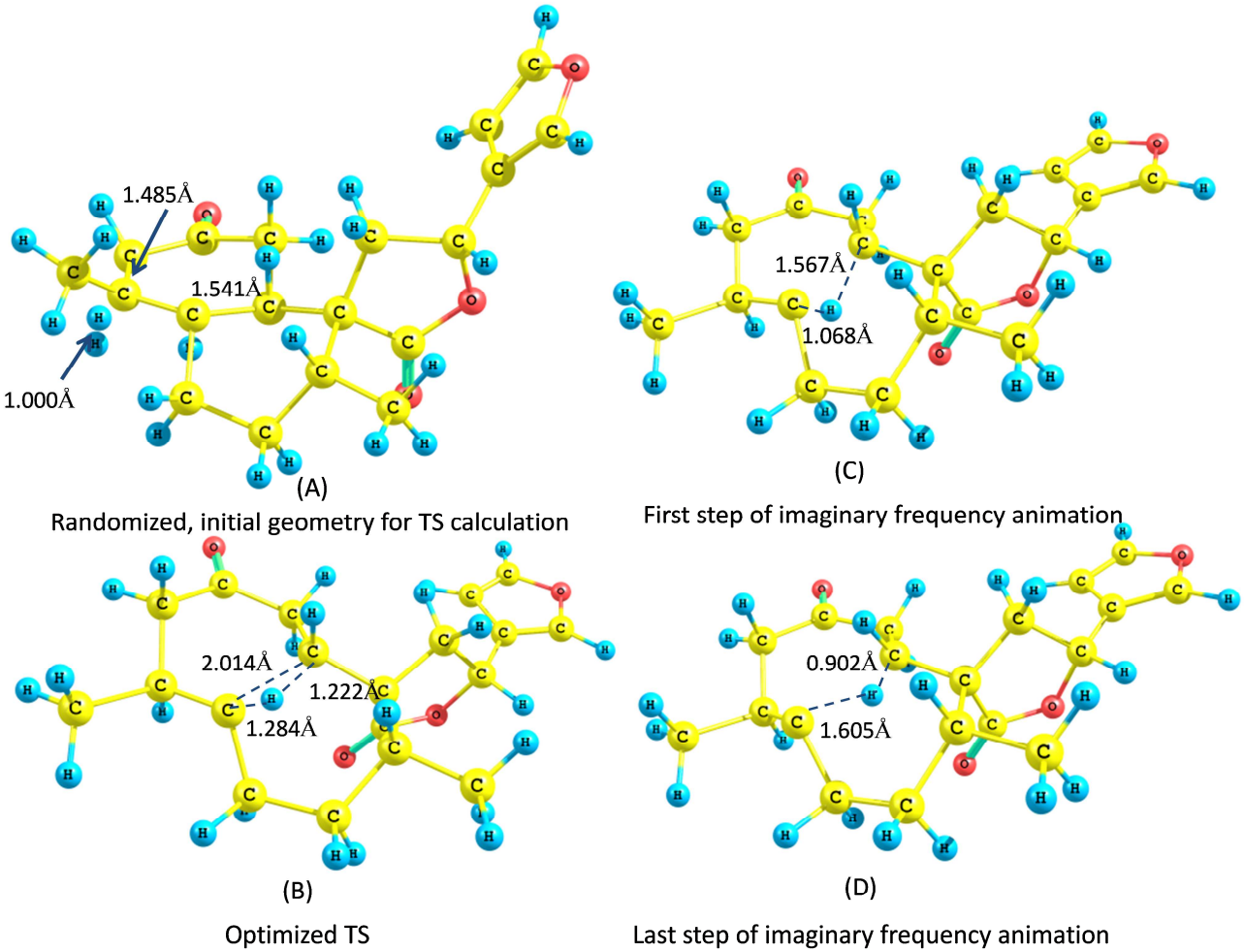

Figure 2. (A) Randomized, initial geometry for TS calculation from optimized *t*-DCTN and hydrogen molecules; (B) corresponding optimized TS geometry; (C) first step of imaginary frequency animation of TS geometry; (D) last step of imaginary frequency animation of TS geometry. Dashed lines represent interatomic distance.

Figure 3 shows the decalin system chair conformation of the *t*-DCTN, with $\Delta^{3,4}$ double bond diastereotopic *Si* face hindered by the axial H-1 and H-5 hydrogens, while for *Re* face, there is no such a hindrance. Thus, H_2 *Re* face approximation is preferable for this reaction affording a highly stereospecific synthetic reduction. Then, DFT calculations is in agreement with the experimental result of highly stereospecific hydrogenation reaction from *t*-DCTN decalin double bond to form exclusively 4(*R*)-*t*-CTN diastereoisomer derivative of CTN-clerodane compound.

The confirmation of the *t*-CTN semi-synthetic derivative can be proved by the absence of absorption around 5,89 ppm (H-3), which is a typical absorption for a vinyl hydrogen, observed in the ^{1}H NMR spectra of the source molecule *t*-DCTN [13]. In fact, for *t*-CTN derivative the H-3 absorption appears in a higher field (around 2 ppm). Furthermore, H-5 and Me-18 follows the same tendency, with *t*-DCTN absorptions in a lower field, compared to the same absorptions of the semi-synthetic *t*-CTN. Specifically for H-5, geometrical theoretical data corroborate with its experimental ^{1}H NMR data. The interatomic distance between H-5 and the unsaturated bond of the C=O (C-20) moiety for *t*-DCTN is smaller than the observed for *t*-CTN (2.455 and 2.549 Å, respectively), indicating the major influence of diamagnetic anisotropic effect of this unsaturation over H-5 for *t*-DCTN. In addition, there is an extra diamagnetic anisotropy from the double bond C=C type ($\Delta^{3,4}$ unsaturation) of the *t*-DCTN. Comparatively, it was observed at δ 3.18 (*m*, 12.50, 10.70, 3.35, 1.20, 1.19 Hz) H-5 absorption for *t*-DCTN and at higher absorption field δ 2.05 (*dddd*, 11.07, 10.64, 10.58, 3.80 Hz) for H-5 of *t*-CTN. On the other hand, the diamagnetic anisotropic effect of the $\Delta^{3,4}$ unsaturation is the main reason for the differences in absorption of Me-18 [δ 1,06 *d* (6.41 Hz) for *t*-CTN; δ 1,97 *dd* (1,27 and 1.20 Hz) for *t*-DCTN] [13]. Moreover, ^{13}C NMR data confirmed the very different absorptions related to C-3, being *t*-CTN in a higher field, according to its less electronegative carbon feature [δ 49.79 for *t*-CTN; 126.73 for *t*-DCTN].

Mass spectrometry data also provided valuable information for structural characterization and confirmation of *t*-CTN derivative, which presented molecular ion peak with *m/z* ratio 316, corresponding

to the molecular mass of *t*-CTN. Additionally, it was observed typical fragments already described for clerodanes skeleton [25], such as base peak with *m/z* ratio 94.

In the second step of the synthetic process, the reduction of the semi-synthetic *t*-CTN in the presence of $NaBH_4$ ethanol solution afforded *t*-CTN-OL epimeric mixture (Scheme 1) as new clerodane compounds. The ^1H NMR data of the crude material indicated a major quantity of the α-OH positioned epimeric alcohol over the β-OH (2.81:1.00 ratio) observed by the area integration of some specific absorptions, as one can see in the absorptions of the methyl group attached at C-18 position (Me-18 absorption as a doublet signal at 0.98 and 0.92 ppm). This experimental observation is corroborated by theoretical calculations shown ahead.

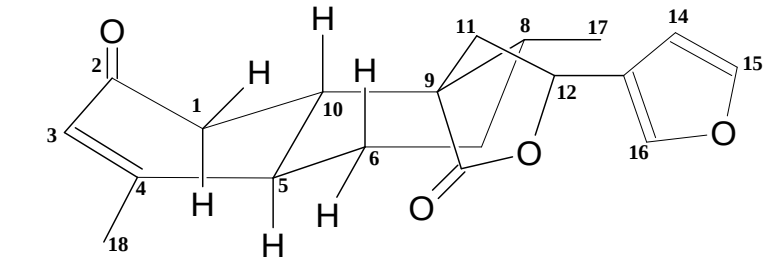

***t*-DCTN**

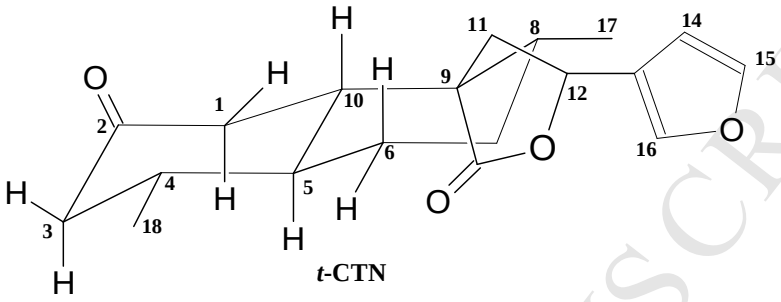

***t*-CTN**

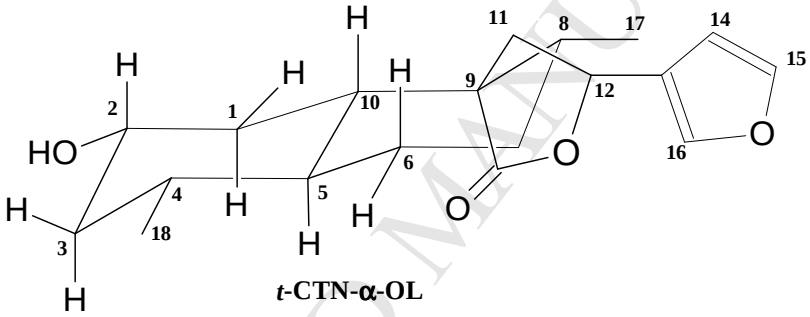

***t*-CTN-α-OL**

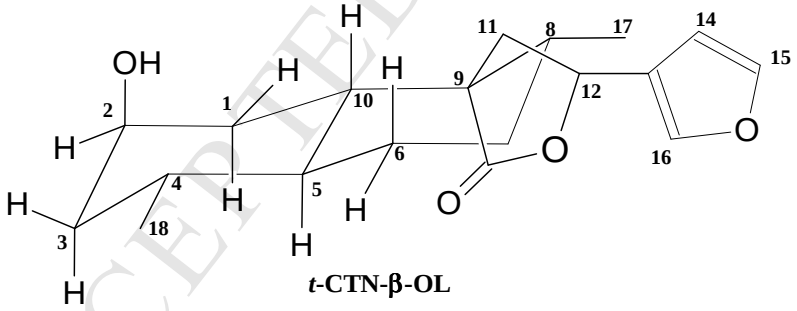

***t*-CTN-β-OL**

Figure 3. Chair conformation representation of *t*-DCTN and its semi-synthetic derivatives *t*-CTN, *t*-CTN-α-OL and *t*-CTN-β-OL.

Figure 4 depicts the optimized geometries of *t*-DCTN, *t*-CTN, *t*-CTN-β-OL and *t*-CTN-α-OL along with C-3 and C-4, C-2 and C-3 and C=O(C-2) bond lengths in Angstroms. On going from *t*-DCTN to *t*-CTN, there is an increase of C-2 and C-3 bond length. Furthermore, this same bond increases from *t*-CTN to *t*-CTN-OL. The increasing trend of C-2 and C-3 from *t*-DCTN to *t*-CTN and to *t*-CTN-OL is according

to C-2 and C-3 sp^2-type hybridization for *t*-DCTN, sp^3-type and sp^2-type hybridizations for C-3 and C-2, respectively, in *t*-CTN, and sp^3-type hybridization for both corresponding carbons in *t*-CTN-OL.

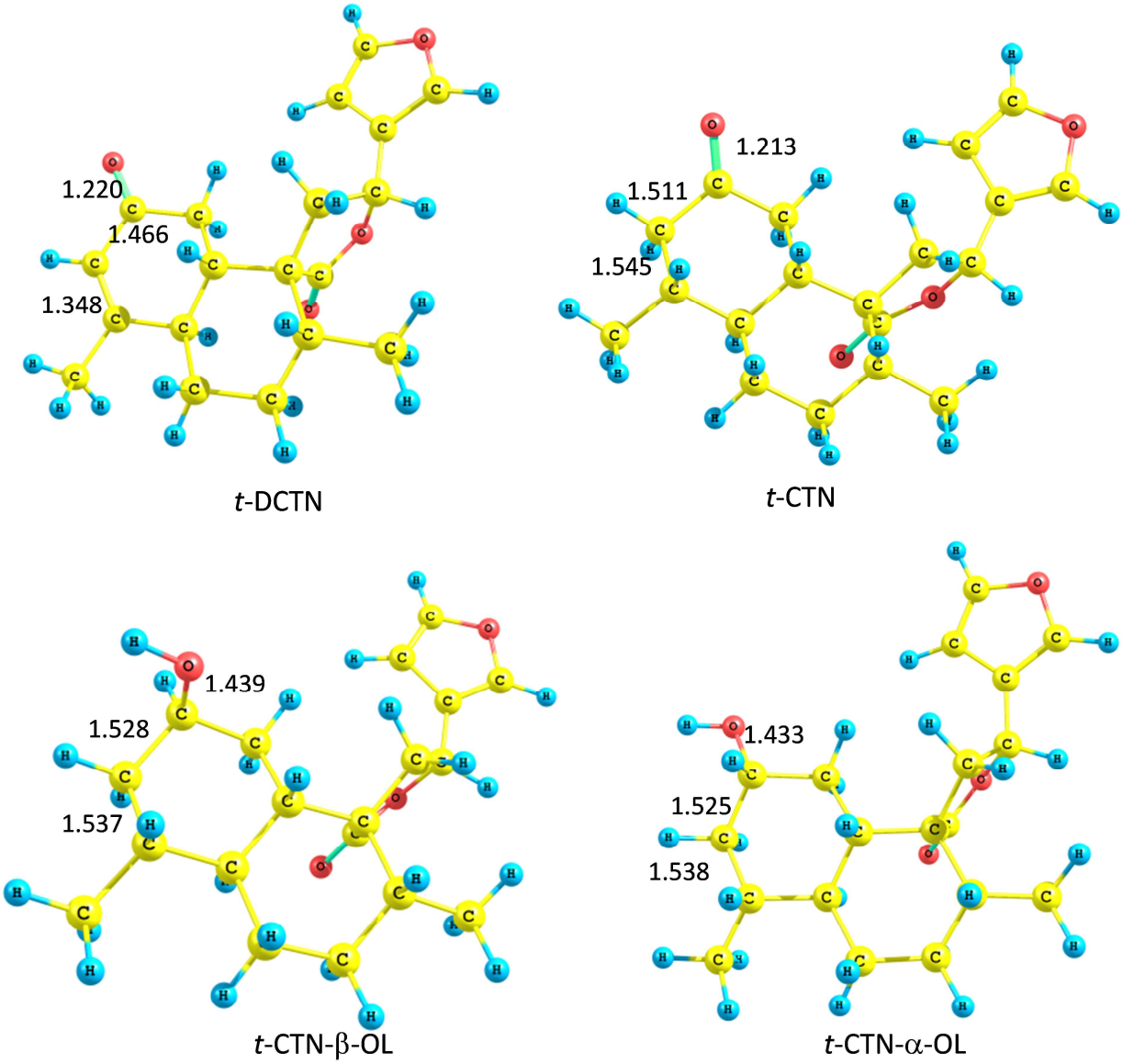

Figure 4. Optimized structures (B3LYP/6-311G++(d,p) level of theory) of *t*-DCTN, *t*-CTN, *t*-CTN-β-OL and *t*-CTN-α-OL and some selected bond lengths, in Angstroms.

In order to explain the stereoselectivity of the *t*-CTN-OL in the presence of $NaBH_4$/EtOH, a theoretical calculation was proceeded to determine its transition states. After several attempts it was observed that the transition state has an ethanol molecule attached to the boron atom of the $NaBH_4$ as its

hydride ion is transferred to the decalin carbonyl carbon. The ethanol molecule decreases the electrophilicity of boron hydride after the hydride ion migration (Figure 5). Table 1 shows the enthalpy of activation (ΔH_{act}) and the electronic energy of activation (ΔE_{act}) for both attacks on *Si* and *Re* faces. According to Boltzmann distribution, the $NaBH_4$ reduction in ethanol medium favors the *t*-CTN-α-OL compound formation in a 1.59:1.00 ratio. According to the calculated energy barrier, the ethanol/$NaBH_4$ attack on *Re* face is 2.76 kcal mol^{-1} more favorable (Table 1). Although, both experimental and theoretical results agree qualitatively, the *t*-CTN-α-OL: *t*-CTN-β-OL theoretical ratio is smaller than that observed by NMR (2.81:1.00).

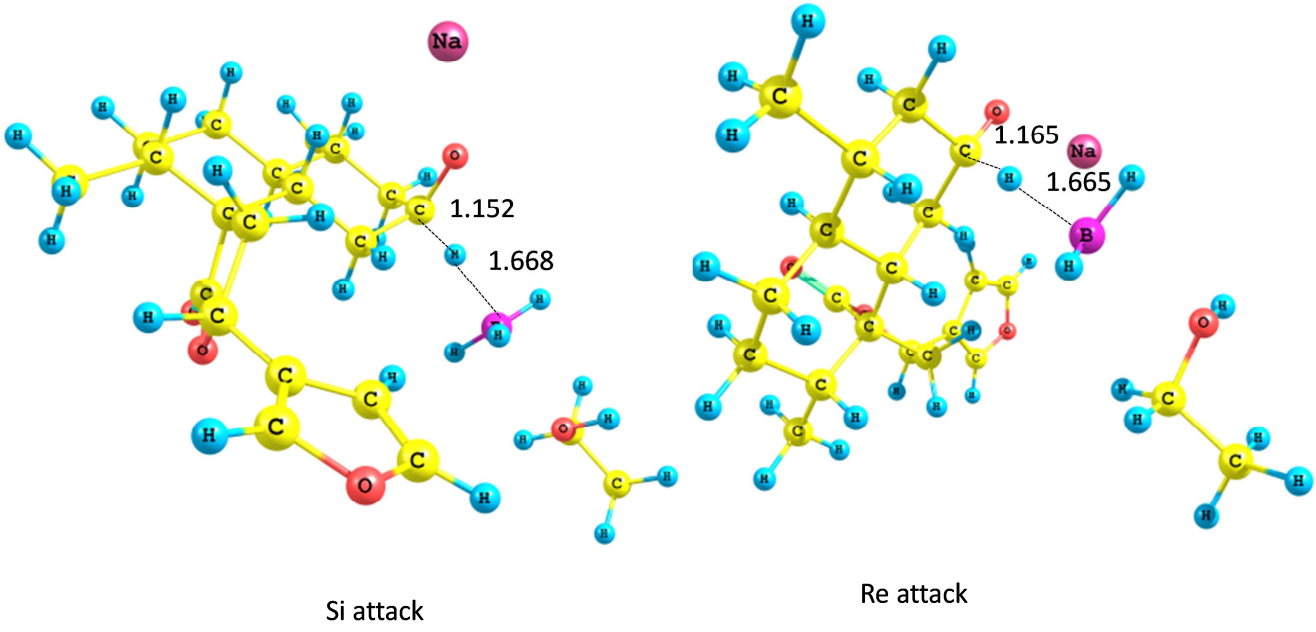

Figure 5. Optimized geometries of transition states from ethanol/$NaBH_4$ reduction of C-2 carbonyl moiety of *t*-CTN from *Si* and *Re* diastereotopic faces approaches. Selected interatomic distances in Angstroms are depicted in dashed lines.

Table 1. Activation electronic energy, E_{act}, and activation entalphy energy, H_{act}, in kcal mol^{-1}, from ωB97XD /6-31G++(d,p) level of theory for borohydride reduction by both diastereotopic faces of *t*-CTN carbonyl.

$NaBH_4$ approach	$\boldsymbol{H_{act}}$ / kcal mol^{-1}	$\boldsymbol{E_{act}}$ / kcal mol^{-1}
Si face	26.92	25.67
Re face	24.16	22.90
Δ	2.76	2.76

The ^{1}H and ^{13}C NMR data related to the elucidation of the new epimeric mixture named *t*-CTN-OL and the semi-synthetic *t*-CTN is found in Table 2. The analysis of the alcohol semi-synthetic derivatives *t*-CTN-α-OL and *t*-CTN-β-OL were compared with the NMR assignments of *t*-CTN structural characterization. The hydrogen absorption at δ 3.50, as well as absorptions at δ 4.18 corresponds to OH group of *t*-CTN-α-OL and *t*-CTN-β-OL, confirming the C-2 carbonyl reduction of *t*-CTN structure.

The secondary methyl group attached to carbon-18 (Me-18) for *t*-CTN is observed at δ 1.06 (a dublet signal with J = 6.48 Hz) while the ^{1}H RMN data of the epimeric mixture shows this chemical shift at higher field δ 0.98 (*d*, J = 5.76 Hz) for *t*-CTN-α-OL and 0.92 (*d*, J = 6.36 Hz) for *t*-CTN-β-OL. Since the carbon-2 for epimeric compounds became sp^3, there is an important geometric difference in the ring A of the decalin moiety which reinforces the diamagnetic anisotropy effect C-20 carbonyl group from the double bond of the lactone ring.

The differences in the assignments of hydrogen atoms H-1, H-3 and H-4, for *t*-CTN and *t*-CTN-OL are derived from the different electronegativity of O-C2/C-2 in these compounds, in which C-2 for *t*-CTN has sp^2-type hybridization and for *t*-CTN-OL epimeric derivatives C-2 become sp^3-type hybridization.

Regarding to ^{13}C NMR comparative data, C-2 chemical shift value for epimeric mixture are observed in a higher field than C-2 of *t*-CTN, confirming the reduction pattern from carbonyl moiety (δ 209.53) to alcohol function (δ 70.09 for *t*-CTN-α-OL and δ 66.69 for *t*-CTN-β-OL).

Table 2. NMR spectroscopic data for semi-synthetic *t*-CTN, *t*-CTN-α-OL and *t*-CTN-β-OL (400 MHz, $CDCl_3$).

position	***t*-CTN**		***t*-CTN-α-OL**		***t*-CTN-β-OL**	
	δ_C, type	**δ_H (*J* in Hz)**	**δ_C, type**	**δ_H (*J* in Hz)**	**δ_C, type**	**δ_H (*J* in Hz)**
1[a]	43.3, CH_2	2.20-2.13	37.1, CH_2	2.10-2.03	34.1, CH_2	2.10-2.03
1e		2.49 tt (13.0, 2.6)		2.49 tt (13.0, 2.6)		2.45-2.38
2	209.5, C		70.0, CH	3.59-3.52	66.6, CH	3.59-3.52
3[a]	49.7,CH_2	2.20-2.13	44.7, CH_2	2.10-2.03	44.7, CH_2	2.10-2.03
3e		2.36 ddd		2.45-2.38		2.45-2.38
4	38.6, CH	1.48-1.38	36.2, CH	1,37-1,26	31.8, CH	1,37-1,26
5	41.6, CH	2.05 dddd (11.0, 10.6, 10.5, 3.8)	41.7, CH	2.10-2.03	41.7, CH	2.10-2.03
6[a]	29.7, CH_2	0.94 dddd (13.0, 12.5, 3.6)	29.9, CH_2	2.10-2.03 m	29.9, CH_2	0.83 dddd (13.0, 12.5, 12.6, 3.6)
6e		2.20-2.13		1.97-1.88		1.97-1.88
7[a]	29.4, CH_2	1.76 dddd (13.0,13.0, 12.7, 3.4)	29.5, CH_2	1.74 dddd (13.0, 12.7, 12.6, 3.4)	29.5, CH_2	1.79-1.69
7e		1.59 m		1.67-1.51		1.67-1.51
8	42.1, CH	1.67 *m*	42.2, CH	1.67-1.51	42.2, CH	1.67-1.51
9	52.3, C		51.8, C		51.7, C	
10	48.4, CH	1.51-1.44	46.7, CH	1.67-1.51	46.8, CH	1.67-1.51
11[a]	40.9, CH_2	2.42 dd (13.0, 8.6)	41.6, CH_2	2.45-2.38	41.6, CH_2	2.45-2.38
11b		2.32 t (8.6)		2.42-2.40 (8.6)		2.45-2.38
12	72.3, CH	5.41 t (8.6)	72.1, CH	5.40 t (8.8)	72.1, CH	5.38 t
13	125.1, C		125.5, C		125.5, C	
14	108.0, CH	6.38 t (1.2)	108.2, CH	6,43 m	108.2, CH	6.41 t (1.2)
15	144.2, CH	7.45	144.0, CH	7,47	143.9, CH	7,47
16	139.3, CH	7.45	139.8, CH	7,47	139.8, CH	7,47
17	17.7, CH_3	1.15 d (6.7)	17.7, CH_3	1.12 d (6.7)	17.8, CH_3	1.11 *d* (6.7)
18	19.6, CH_3	1.06 d (6.4)	19.4, CH_3	0.98 d (5.7)	19.3, CH_3	0.92 *d* (6,3)
OH				4,18[†]m		3.50[†]br s
20	177.0, C		177.4, C		177.4, C	

For hydrogens 1, 3, 6, 7 "**a**" refers to axial position and "**e**" to equatorial position.
Overlapped signals are reported without designating multiplicity.
All ^1H assignments confirmed throught 2D NMR data.
[†]Values can be exchanged.

Mass spectrometry data also provided valuable information for structural characterization confirmation of epimeric mixture. It was found the molecular ion peak with *m/z* ratio 318, which is the exactly molecular mass for both *t*-CTN-α-OL and *t*-CTN-β-OL. Moreover, typical fragments already described for clerodane skeleton [25], such as base peak with *m/z* ratio 95 for *t*-CTN-β-OL and *m/z* ratio 161 for *t*-CTN-α-OL were also presented in mass spectra data.

In a previous work, we investigated the magnetic, electronic and geometrical properties of the bioactive clerodane *t*-DCTN by means of a theoretical-experimental comparative analysis, in order to give full support for the NMR characterization of natural products [12]. In this work we studied the NMR chemical shifts and coupling constants for the new semi-synthetic *t*-CTN, *t*-CTN-β-OL and *t*-CTN-α-OL compounds by applying the same previously developed protocol.

Figures S9 and S10 gives excellent determination coefficients (R^2 above 0.97) for plots between experimental and theoretical (B3LYP/6-311G++(d,p)) ^{1}H NMR and ^{13}C NMR chemical shifts, in ppm, of *t*-CTN-α-OL and *t*-CTN-β-OL, respectively.

As to *t*-CTN, Figure S11 depicts the correlations between the experimental ^{1}H NMR/^{13}C NMR chemical shifts data previously performed for *t*-CTN [13] and the theoretical ^{1}H NMR/^{13}C NMR data obtained herein for *t*-CTN in which it was observed very good linear correlations (both R^2 above 0.990). In fact, the B3LYP/6-311G++(d,p)/GIAO method confirmed its precision to describe magnetic properties of low symmetry and flexible structures similar to diterpene compounds [12].

Concerning the comparative analyses of coupling constants for natural *t*-CTN, it was found in Figure S12 two points (related to couplings involving H-4/Me-18 and H-5/Me-17) out of the line. These couplings are from single hydrogen and methyl group. Due to free rotation of the methyl group, methylic hydrogen coupling with the single hydrogen is equivalent. On the other hand, the dynamic free rotation of methylic hydrogen atoms is not observed in theoretical stationary calculation, which could explain this observed discrepancy.

Figures S13a and S13b show the plots of experimental and theoretical coupling constants versus corresponding delocalization index of vicinal or long range protons of *t*-CTN, respectively. Both of them showed a reasonably good coefficient of determination (R^2=0.9441 and 0.9587, respectively), confirming that the amount of shared charge density between long or vicinal protons is related with the magnitude of the corresponding coupling constant [26], i.e., there is a relation between electronic and magnetic properties of *t*-CTN as shown in Figure S13a. Moreover, the same two points related to hydrogens H-4/H-18 and H-8/H-17 are also out of the trend line (Figure S13) which is in accordance with the same theoretical-experimental discrepancy observed in Figure 7 and it can be similarly reasoned on the same grounding as done above. The theoretical and experimental results from Figures S11-S13 are important to confirm the structure and the most stable conformation of semi-synthetic *t*-CTN. These results reinforce the experimental NMR elucidation of semi-synthetic *t*-CTN.

In order to investigate possible intramolecular interactions in the molecular structure of *t*-CTN which could account for its most stable and experimentally observed conformation, we used QTAIM calculations [27] based on the gradient of the charge density distribution to carry out its topological analysis. The topology of charge density may have four types of critical points: the nuclear attractor critical point (in which atomic nucleus is located), the bond critical point (a critical point between two linking atoms), the ring critical point (a critical point within a ring) and the cage critical point (a critical point inside a molecular cage). Specifically, a critical point is a mathematical point of a determined function, whose gradients, with respect to their coordinates, are zero. The bond path is an atomic interaction line linking two nuclear critical points (or atomic basins) and one bond critical point between them. It corresponds to the maximum charge density compared to vicinal transversal region. Figure 6 shows the molecular graph (a set of critical points of the charge density and bond paths) for *t*-CTN.

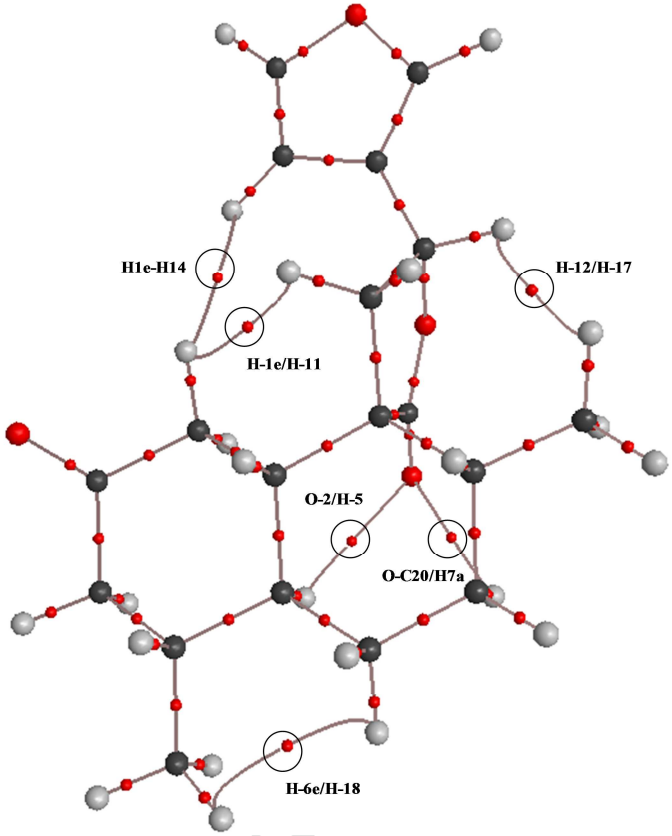

Figure 6. Molecular graph for *t*-CTN.

The quantum theory of atoms in molecules can be used to quantify and qualify bonded interactions [28,29] as shared interaction (covalent bond) or closed shell interaction (ionic bond, van der Waals interaction, hydrogen bond) based on the value of the charge density of the critical point (ρ_b); the value and the sign of the Laplacian ($\nabla^2\rho$) of the charge density; the ratio $|\lambda_1|/\lambda_3$, where λ_1 and λ_3 are eigenvalues of Hessian matrix of the charge density; the ratio G_b/ρ_b, where G_b is the kinetic energy density; and the total energy density (H_b) at the bond critical point. A closed shell interaction is characterized by positive values of Laplacian $\rho(r)$ which indicates the domination of the positive contribution to the Hessian matrix trace. The trace of diagonalized Hessian matrix eigenvalues is equal to the Laplacian of the electron density in this critical point. The ratio $|\lambda_1|/\lambda_3$ <1, the ratio G_b/ρ_b>1 or

close to 1, and H_b with a positive value, close to zero corroborates this features, meaning physically as charge depletion.

Table 3 shows these six topological data for all intramolecular bonded interactions for the most stable conformer of *t*-CTN. All values in Table 3 are in agreement with those corresponding values for *t*-DCTN in a previous work, namely the five out of the six H—H / (C)O--H(C) intramolecular interactions in *t*-CTN (which are also found in *t*-DCTN) and they are characterized as closed shell interactions [12]. There is an additional intramolecular interaction (H—H bond) found for *t*-CTN between H-6, located in equatorial position, and one of the hydrogens of Me-18 (See Figure 6). The H—H bond was shown to exist in alkane complexes [30]. This structural feature might be associated with different reactivity behavior between these two clerodanes in the presence of $NaBH_4$ [31].

Table 3. Values of the charge density of bond critical points (ρ_b). the corresponding Laplacian of the charge density ($\nabla^2\rho$), in a.u., the ratio $|\lambda_1|/\lambda_3$, the ratio G_b/ρ_b, and the total energy density (H_b), in a.u., of all intramolecular bonded interactions from molecular graph of *t*-CTN.

Interactions	$\rho_b x10^2$/a.u.	$\nabla^2\rho$	$\lvert\lambda_1\rvert/\lambda_3$	G_b/ρ_o	$H_b x10^2$/a.u.
H-1e/H-11	1.293	0.045	0.194	0.722	0.202
H-1e-H-14	0.370	0.011	0.174	0.635	0.052
H-17-H-12	0.827	0.028	0.165	0.701	0.123
H-6e-H-18	1.090	0.044	0.162	0.807	0.209
OC-20/H-7a	0.901	0.030	0.170	0.723	0.092
OC-20/H-5	0.977	0.031	0.175	0.711	0.086

Theoretical ^1H and ^{13}C NMR chemical shifts were also calculated for both epimeric derivatives (*t*-CTN-α-OL and *t*-CTN-β-OL). The values of the coefficient of determination for experimental/theoretical chemical shifts of both compounds of epimeric mixture showed satisfactory correlation (Figures S14 and S15).

There is a number of *Croton cajucara* Benth researches devoted to its chemical, biochemical, pharmacological and more recently potential advantages of molecular incorporation into drug delivery systems, specifically *t*-DCTN-load studies. Since 19-*nor*-clerodane-type diterpenes has being largely investigated this present work draws significant attention towards the simple semi-synthetic procedure to obtain highly stereospecific *t*-CTN in which some biological activities were discovered. Moreover, $NaBH_4$ ethanol reduction of *t*-CTN gives an unknown epimeric mixture *t*-CTN-α-OL / *t*-CTN-β-OL in which future physical chemical and pharmacological studies will be needed. This work mainly shows that both proposed synthesis yield highly selective 19-*nor*-clerodane-type diterpene derivatives rather than several adducts. In addition, theoretical and experimental characterization of the adducts from this work has been successfully applied where DFT and QTAIM methods (whose approach has been previously applied to *t*-DCTN) are valuable tools to assist experimental determination of the 19-*nor*-clerodane-type diterpenes.

5. Conclusions

The catalytic hydrogenation as synthetic methodology applied to obtain *t*-CTN has been confirmed as a reproducible methodology, representing an important alternative to catalytic reduction reactions lacking the need of using hydrogenation equipment. This reaction is highly stereospecific affording exclusively 4(*R*)-*t*-CTN, the natural *t*-CTN diastereoisomer, which was confirmed by DFT calculations. Reduction of *t*-CTN derivative using $NaBH_4$ in ethanolic solution afforded epimeric mixture of *t*-CTN-OL in a major proportion for α-OH compound over β-OH derivative (2.81:1.0), which was somewhat confirmed by DFT. Theoretical study showed that one ethanol molecule explicitly participates in the transition state of $NaBH_4$ reduction of *t*-CTN.

A theoretical protocol previously developed and applied to *t*-DCTN was validated for natural *t*-CTN structure and for *t*-CTN-OL epimeric mixture. Moreover, QTAIM delocalization indexes involving vicinal or long range protons correlates well with both corresponding theoretical and experimental spin-spin coupling constants for natural *t*-CTN, indicating that the amount of charge

density between each proton pair (being vicinal or not) are directly proportional with the spin-spin coupling constant. Additionally, from the analysis of topological data there are six intramolecular interactions for *t*-CTN, indicating a different pattern of flexibility of this molecule compared to its precursor *t*-DCTN.

Acknowledgments

The authors thank FAPERN (Fundação de Amparo à Pesquisa do Estado do Rio Grande do Norte), CAPES (Coordenação de Aperfeiçoamento de Pessoal de Nível Superior) and CNPq (Conselho Nacional de Desenvolvimento Científico e Tecnológico) for financial support.

References

[1] W.R. Chan, D.R. Taylor, C.R. Willis, Chem. Commun. 4 (1967) 191-191.
[2] W.R. Chan, D.R. Taylor, C.R. Willis, J. Chem. Soc. C Org. (1968) 2781–2785.
[3] J.F. Blount, W.R. Chan, J. Clardy, P.S. Manchand, J.O. Pezzanite, J. Chem. Res. Synopses. 4 (1984) 114–115.
[4] M.A.M. Maciel, A.C. Pinto, A.C. Arruda, S.G.S.R. Pamplona, F.A. Vanderlinde, A.J. Lapa, A. Echevarria, N.F. Grynberg, I.M.S. Cólus, R.A.F. Farias, A.M. Luna Costa, V.S.N. Rao, J. Ethnopharmacol. 70 (2000) 41–55.
[5] M.A.M. Maciel, J.R. Martins, A.C. Pinto, C.R. Kaiser, A. Esteves-Souza, A. Echevarria, J. Brazilian Chem. Soc. 18 (2007) 391–396.
[6] C.A. Hiruma-Lima, W. Toma, J. de Souza Gracioso, A.B.A. de Almeida, L.M. Batista, L. Magri, A.C.B. de Paula, F.R. Soares, D. S. Nunes, A.R.M. Souza Brito, Biol. Pharm. Bull. 25 (2002) 452–456.
[7] F.F. Perazzo, J.C.T. Carvalho, M. Rodrigues, E.K.L. Morais, M.A.M. Maciel, Rev. Bras. Farmacogn. 17 (2007) 521–528.
[8] P.M. Mirzayans, R.H. Pouwer, C.M. Williams, P.V. Bernhardt, European J. Org. Chem. 8 (2012) 1633–1638.
[9] P.S. Melo, N. Durán, M. Haun, Toxicology. 159 (2001) 135–141.
[10] P.S. Melo, N. Durán, M. Haun, Hum. Exp. Toxicol. 21 (2002) 281–288.
[11] H. Itokawa, Y. Ichihara, H. Kojima, K. Watanabe, K. Takeya, Phytochemistry. 28 (1989) 1667–1669.
[12] B.A. Soares, C.L. Firme, M.A.M. Maciel, C.R. Kaiser, E. Schilling, A.J. Bortoluzzi, J. Braz. Chem. Soc. 25 (2014) 629–638.
[13] M.A.M. Maciel, A.C. Pinto, C.R. Kaiser, Magn. Reson. Chem. 41 (2003) 278–282.

[14] R. Fletcher, Practical Methods of Optimization: Constrained optimization, J. Wiley, 1981.
[15] A.D. Becke, J. Chem. Phys. 98 (1993) 1372–1377.
[16] A.D. Becke, J. Chem. Phys. 98 (1993) 5648–5652.
[17] C. Lee, W. Yang, R.G. Parr, Phys. Rev. B. 37 (1988) 785–789.
[18] M. Head-Gordon, J.A. Pople, M.J. Frisch, Chem. Phys. Lett. 153 (1988) 503–506.
[19] T.H. Dunning, J. Chem. Phys. 90 (1989) 1007–1023.
[20] M.J. Frisch, M. Head-Gordon, J.A. Pople, Chem. Phys. Lett. 166 (1990) 281–289.
[21] E. Cancès, B. Mennucci, J. Tomasi, Chem. Phys. 107 (1997) 3032–3041.
[22] B. Mennucci, J. Tomasi, J. Chem. Phys. 106 (1997) 5151–5158.
[23] M.J. Frisch, G.W. Trucks, H.B. Schlegel, G.E. Scuseria, J.R. Cheeseman, M.A. Robb, G. Scalmani, V. Barone, B. Mennucci, G.A. Petersson, H. Nakatsuji, M. Caricato, X. Li, H.P. Hratchian, A.F. Izmzylov, J. Bloino, G. Zheng, J.L. Sonnenberg, M. Hada, M. Ehara, K. Toyota, R. Fukuda, J. Ishida, M. Hasegawa, T. Nakajima, Y. Honda, O. Kitao, H. Nakai, T. Vreven, J.A. Montgomery Jr., J.E. Peralta, F. Ogliaro, M. Bearpark, J.J. Heyd, E. Brothers, K.N. Kudin, V.N. Staroverov, R. Kobayashi, J. Normand, A. Raghavachari, A. Rendell, J.C. Burant, S.S. Iyengar, J. Tomasi, M. Cossi, N. Rega, J.M. Millan, M. Klene, J.E. Knox, J.B. Cross, V. Bakken, C. Adamo, J. Jaramillo, R. Gomperts, R.E. Stratmann, O. Yazyev, A.J. Austin, R. Cammi, C. Pomelli, J.W. Ochterski, R.L. Martin, K. Morokuma, V.G. Zakrzewski, G.A. Voth, P. Salvador, J.J. Dannerberg, S. Dapprich, A.D. Daniels, J. Farkas, B. Foresman, J.V. Ortiz, J. Cioslowski, D.J. Fox, GAUSSIAN 09, Revision, Gaussian, Inc., Wallingford, CT, 2009
[24] J. Biegler-König, F. Schönbohm, AIM2000, 2002.
[25] M.A.M. Maciel, R.S. Leal, T.N.C. Dantas, V.F. Veiga Jr., Rev. Fitos. 3 (2007) 37–45.
[26] C.F. Matta, J. Hernández-Trujillo, R.F.W. Bader, J. Phys. Chem. A. 106 (2002) 7369–7375.
[27] R.F.W. Bader, Atoms in Molecules: A Quantum Theory, Oxford University Press, Incorporated, Clarendon Press: Oxford, 1990.
[28] S.J. Grabowski, Chem. Rev. 111 (2011) 2597–2625.
[29] C.F. Matta, J. Hernández-Trujillo, T.H. Tang, R.F.W. Bader, Chemistry. 9 (2003) 1940–1951.
[30] N.K.V. Monteiro, C.L. Firme, J. Phys. Chem. A. 118 (2014) 1730–1740.
[31] M.A.M. Maciel, F.E.S. Gomes, B.A. Soares, N.F. Grynberg, A. Echevarria, I. M. S. Cólus, C.R. Kaiser, W.A. Morais, N.S.S. Magalhães, Bioactive Phytochemicals: Perspectives for Modern Medicine, Vol. 2, in: V.K. Gupta (Ed), Biological Effectiveness and Recent Advancing of Natural Products on the Discovery of Anticancer Agents, Daya Pulishing House, Nova Delhi, 2013, pp. 239-293.

Highlights

- Highly stereospecific hydrogenation from *t*-DCTN to form 4(*R*)-*t*-CTN diastereoisomer
- $NaBH_4$/ethanol reduction of *t*-CTN affording *t*-CTN-OL epimeric mixture
- Most stable conformer of *t*-CTN has six intramolecular bonded interactions